RESEARCH INTO ADVANCED CONCEPTS

OF MICROWAVE POWER AMPLIFICATION

AND

GENERATION UTILIZING LINEAR BEAM DEVICES

P. R. McIsaac

School of Electrical Engineering

Cornell University

Semiannual Status Report

June 1971

Research Grant NGL 33-010-047 No. 2

National Aeronautics and Space Administration

Office of Grants and Research Contracts
Code SC
Washington, D. C. 20546

ABSTRACT

This is an interim report which summarizes work during the past six months on a theoretical study of some aspects of the interaction between a drifting stream of electrons with transverse cyclotron motions and an electromagnetic field. Particular emphasis is given to the possible generation and amplification of millimeter waves. This report includes a discussion of large signal effects in cyclotron resonance oscillators, with particular attention given to the power saturation mechanism.

INTRODUCTION

The objective of this research program is to explore theoretically some aspects of the interaction between a drifting stream of electrons having transverse cyclotron motions and an electromagnetic field; particular emphasis being given to the possible generation and amplification of millimeter waves. Because of the interest in possible applications to millimeter wavelengths, this study concentrates on electron stream-electromagnetic field interactions which involve an uniform, or fast-wave, circuit structure or cavity of simple shape.

An investigation of the large signal effects in cyclotron resonance oscillators has been performed. A digital computer was used to obtain numerical results for a particular set of oscillator parameters. The primary aim of the investigation was to explore the mechanism which produces power output saturation in a cyclotron resonance oscillator. This large signal analysis is discussed in the following section, which is a preprint of a paper accepted for publication in the International Journal of Electronics.

SATURATION EFFECTS IN CYCLOTRON RESONANCE OSCILLATORS

J. F. Rowe, Jr.
School of Electrical Engineering
Cornell University
Ithaca, New York 14850

ABSTRACT

This paper presents the results of a large signal analysis of a cyclotron resonance oscillator. A digital computer was used to obtain numerical results for a particular set of parameters. The model adopted for the oscillator assumes a spiraling filamentary electron beam interacting with a rectangular cavity. Both the gain and saturation mechanisms for a cyclotron resonance oscillator are discussed.

List of Principal Symbols

a	- waveguide width
B_o	- DC axially directed magnetic field
$\underset{\sim}{B}$	- total RF magnetic field
c	- velocity of light
e	- charge of electron
$\underset{\sim}{E}$	- total RF electric field
E_o	- peak RF electric field strength in dielectric
I_o	- DC beam current
$\underset{\sim}{J}$	- current density vector
k_1, k_2	- propagation constants
m_o	- electron rest mass
Q_x	- external Q
R	- energy balance factor
t	- time
U	- impedance mismatch factor
$\underset{\sim}{v}$	- total beam velocity
V_o	- DC beam voltage
$v_{nx,y,z}$	- n^{th} order Fourier components for x, y, and z velocities
v_{to}	- transverse velocity
x,y,z	- rectangular coordinate system
x', y'	- $(x + a/2)$, $(y + a/2)$
v_{zo}	- axial velocity
Z_1, Z_2	- waveguide impedances
β_c	- beam cyclotron wave number
ε_o	- permittivity of free space

ϵ_r	- relative permittivity of dielectric
η	- impedance of free space = $(\mu_o/\epsilon_o)^{\frac{1}{2}}$
$\dot{\theta}$	- relativistic orbiting radian frequency
λ	- RF field wavelength in cavity
μ_o	- permeability of free space
ρ	- total charge density
τ_n	- n^{th} order Fourier component in charge density expansion
ψ	- conversion efficiency
ω	- RF radian frequency
ω_{co}	- waveguide radian cutoff frequency in TE_{10} mode = $\pi c/a$.

1. INTRODUCTION

Over the past decade much attention has been focused upon devices utilizing the interaction of fast waves with rotating electron beams. Tubes based on this principle, the "Electron Cyclotron Masers" or "Cyclotron Resonance Oscillators," have potential as generators of high power millimeter wavelength radiation. A sequence of such devices has been constructed and reported upon: Chow and Pantell (1960), Hirshfield and Wachtel (1964), Bott (1965), Beasley (1966), Antakov _et al_. (1966), Schriever and Johnson (1966), and Kulke and Wilmarth (1969).

It was shown by Chow and Pantell (1960) that the interaction of rotating charge with the transverse waveguide magnetic field can produce longitudinal bunching and set up conditions for energy transfer to the electromagnetic fields via the $\underset{\sim}{v} \cdot \underset{\sim}{E}_{RF}$ mechanism. Subsequently, Hsu (1966) discovered that the beam-field coupling produces a relativistic electron mass shift which leads to wave growth. Sehn and Hayes (1969) compared the effects of relativistic bunching and transverse magnetic field bunching and concluded that in the hollow beam-TE_{10} waveguide mode interaction, relativistic bunching predominates, particularly near cutoff. Lindsay (1970) supports this conclusion in the case of helical, filamentary beams, and presents evidence that the RF magnetic fields may in fact always oppose the relativistic growth mechanism for the forward wave interaction.

A small signal coupled-mode analysis describing the interaction of a spiraling, filamentary electron beam with the fields of a uniform waveguide has been developed by McIsaac (1968) and extended to predict the start-oscillation conditions of a device with the beam inside a rectangular cavity (McIsaac and Rowe 1970). The model utilizes a filamentary helix of charge with electrons drifting along the cavity axis with axial velocity v_{zo} and rotating about a static magnetic field B_o with transverse velocity v_{to} at radian frequency

$$\dot{\theta} = \frac{eB_o}{m_o}\left[1 - \frac{(v_{to}^2 + v_{zo}^2)}{c^2}\right]^{\frac{1}{2}} . \qquad (1)$$

With the electron orbiting frequency set slightly below cavity resonance, strong coupling between the electron beam and the electromagnetic field occurs, and self-sustaining oscillations are produced. It is found that to obtain oscillations, practically all the beam energy must be incorporated in kinetic energy of rotation.

With the intent of further illuminating the processes at work within cyclotron resonance devices, this paper presents a large signal ballistic analysis of a spiraling, filamentary electron beam interacting with the RF fields of a rectangular, lossless cavity of square cross section. Space charge forces have been neglected, and only the effects of the dominant, degenerate, TE_{101} and TE_{011} modes are considered. The beam radius r_o is much less than the cavity width. As a consequence, the presence of the axial component of the RF magnetic field is ignored, and the transverse RF fields are assumed to be circularly polarized, rotating in the same sense as the charge.

The fields within the cavity satisfy the non-homogeneous wave equations:

$$\nabla^2 \underset{\sim}{E} - \frac{1}{c^2} \frac{\partial^2 \underset{\sim}{E}}{\partial t^2} = \frac{\nabla \rho}{\varepsilon_o} + \mu_o \frac{\partial \underset{\sim}{J}}{\partial t} \tag{2}$$

$$\nabla^2 \underset{\sim}{B} - \frac{1}{c^2} \frac{\partial^2 \underset{\sim}{B}}{\partial t^2} = - \frac{\nabla x \underset{\sim}{J}}{\mu_o} \quad . \tag{3}$$

The homogeneous solutions to these equations are given by the familiar cavity standing-wave fields. Upon introduction of an electron beam into the structure, a non-homogeneous or "driven" solution appears and must be superimposed upon the homogeneous solution to obtain the total field.

The motion of charge within the cavity is governed by the relativistic equation of motion:

$$\frac{d}{dt}\left\{ \frac{\underset{\sim}{v}}{\left[1-\left(\frac{|\underset{\sim}{v}|^2}{c^2}\right)\right]^{\frac{1}{2}}} \right\} = \frac{e}{m_o} \left[\underset{\sim}{E} + \underset{\sim}{v} \times \underset{\sim}{B} + \underset{\sim}{v} \times B_o \underset{\sim}{a}_z\right], \tag{4}$$

where B_o is the axial DC magnetic flux density which produces the spiraling motion of the DC beam.

In the analysis, the continuous beam of Figure 1 is decomposed into a series of discrete charge groups. The Cyclotron Resonance Oscillator is assumed to have settled into steady-state operation, i.e.,

$$f(t + \frac{m2\pi}{\omega}) = f(t), \; m = \pm 1, \pm 2, \ldots \tag{5}$$

for all beam and field quantities, and only those representative charge groups entering the structure over one RF cycle need be considered.

Based upon the fields within an infinite waveguide with a step dielectric discontinuity, a model of the cavity has been devised and will be described in the next sections. With a modulated electron beam in the waveguide, it is possible to generate a condition of zero transverse electric field at a point one-half wavelength distant from the discontinuity. The waveguide can thus be shorted and converted into a resonant cavity.

The helical beam enters the cavity and is acted upon by the homogeneous RF fields. The beam becomes distorted as position modulation appears. A Fourier analysis of beam variables is performed at periodically spaced axial intervals, and based upon certain "slowly varying" assumptions on the Fourier coefficients, approximate closed-form expressions for the non-homogeneous fields can be generated. In this manner, the charge group equations of motion are integrated along the length of the cavity. Oscillation conditions require the maintenance of boundary conditions at both the entrance and exit planes; if these are fulfilled, then the input parameters are consistent with oscillation. However, if the requisite final conditions are not satisfied at the cavity exit, the initial parameters are reset and the integrations repeated until oscillation conditions are achieved.

2. CAVITY STANDING-WAVE PATTERNS

The magnitude of the TE_{101}, standing-wave, transverse electric and magnetic fields of a lossless, closed, rectangular cavity are sketched in Figure 2a. Since the tangential components of E must be zero at the end walls, the electric field exhibits the well-known $\sin(2\pi z/\lambda)$ form.

With a spiraling electron beam in the cavity, non-homogeneous electric fields are generated. The transverse field components must still vanish at the end walls. To yield the required cancelling field, there must be some shift in the resonant frequency of the cavity (Figure 2b).

With this simple physical argument as a point of reference, the fields within an inhomogeneously filled waveguide will be examined and used to produce an idealized cavity model.

3. CAVITY MODEL

A lossless waveguide of square (a x a) cross section is evacuated in the region $z > 0$ and filled with a lossless, non-magnetic dielectric of relative permittivity ϵ_r for $z < 0$. In the evacuated portion, the impedance of the degenerate TE_{10} and TE_{01} modes is

$$Z_1 = \frac{\eta}{\left[1 - \left(\frac{\omega_{co}}{\omega}\right)^2\right]^{\frac{1}{2}}} , \tag{6}$$

and in the dielectric,

$$Z_2 = UZ_1. \tag{7}$$

Such a model is not proposed as being representative of any physical device. This model does allow the large signal interaction within the cavity to be readily analyzed, including the effects of external loading. It is believed, moreover, that this large signal analysis should be applicable to the interpretation of the interaction in actual cyclotron resonance devices with cavities employing an output system of vacuum window and iris, if the Q_x of the model employed here is adjusted to equal the value for the device.

An RF wave comprised of equi-amplitude, and $\pi/2$-phased, TE_{10} and TE_{01} modes propagates in the $-z$ direction and strikes the discontinuity at $z = 0$. The transverse components of the transmitted fields in the dielectric ($z < 0$) are written as

$$E_{2x} = E_o \sin \frac{\pi y'}{a} \cos(\omega t + k_2 z) \tag{8}$$

$$E_{2y} = E_o \sin \frac{\pi x'}{a} \sin(\omega t + k_2 z) \tag{9}$$

$$H_{2x} = \frac{E_{2y}}{Z_2} \tag{10}$$

$$H_{2y} = -\frac{E_{2x}}{Z_2} \tag{11}$$

with

$$k_2 = \frac{\omega \varepsilon_r^{\frac{1}{2}}}{c} \left[1 - \left(\frac{\omega_{co}}{\sqrt{\varepsilon_r}\,\omega}\right)\right]^{\frac{1}{2}}. \tag{12}$$

This wave is the output from the oscillator.

Relative to the transmitted, or "output" field magnitude E_o, the transverse fields in the region $z > 0$ are

$$E_{1x} = \frac{E_o(U+1)}{2U} \sin \frac{\pi y'}{a} \left[\cos(\omega t+k_1 z) + \left(\frac{U-1}{U+1}\right) \cos(\omega t-k_1 z)\right] \tag{13}$$

$$E_{1y} = \frac{E_o(U+1)}{2U} \sin \frac{\pi x'}{a} \left[\sin(\omega t+k_1 z) + \left(\frac{U-1}{U+1}\right) \sin(\omega t-k_1 z)\right] \tag{14}$$

and

$$H_{1x} = \frac{E_o(U+1)}{2UZ_1} \sin \frac{\pi x'}{a} \left[\sin(\omega t+k_1 z) - \left(\frac{U-1}{U+1}\right) \sin(\omega t-k_1 z)\right] \tag{15}$$

$$H_{1y} = -\frac{E_o(U+1)}{2UZ_1} \sin \frac{\pi y'}{a} \left[\cos(\omega t+k_1 z) - \left(\frac{U-1}{U+1}\right) \cos(\omega t-k_1 z)\right] \tag{16}$$

with

$$k_1 = \frac{\omega}{c} \left[1 - \left(\frac{\omega_{co}}{\omega}\right)^2\right]^{\frac{1}{2}} . \tag{17}$$

On the waveguide axis, the RF fields are circularly polarized.

The fields of Equations (13) - (16) are the superposition of the forward and reverse homogeneous transverse solutions to the wave equations. Acted upon by these fields, the beam response is described by Fourier expansions:

$$v_x(z,t) = \sum_{n=0}^{\infty} v_{nx}(z)e^{jn(\omega t - \beta_c z)} \qquad (18)$$

$$v_y(z,t) = \sum_{n=0}^{\infty} v_{ny}(z)e^{jn(\omega t - \beta_c z)} \qquad (19)$$

$$v_z(z,t) = \sum_{n=0}^{\infty} v_{nz}(z)e^{jn(\omega t - \beta_c z)} \quad . \qquad (20)$$

The wave number β_c is defined by the integral

$$\beta_c(z) = \frac{\omega}{2\pi}\,\frac{eB_o}{m_o}\,\frac{1}{v_{zo}(z)}\int_0^{2\pi/\omega}\left[1 - \frac{v^2(z,t)}{c^2}\right] dt \ . \qquad (21)$$

This quantity represents the time-averaged propagation "constant" of spiraling electrons as a function of the axial coordinate.

Because of charge gyration about B_o, the x and y Fourier coefficients are approximately space-periodic and are taken as

$$v_{nx}(z) = u_{nx}(z)\ [-\sin(\beta_c z + \phi)] \qquad (22)$$

$$v_{ny}(z) = u_{ny}(z)\cos(\beta_c z + \phi) \quad . \qquad (23)$$

The charge density function is described by

$$\rho(z,t) = \delta(x)\delta(y)\left[\frac{I_o}{v_{zo}(z)} + \sum_{n=1}^{\infty} \tau_n(z)e^{jn(\omega t-\beta_c z)}\right] . \qquad (24)$$

The δ-functions arise from the filamentary nature of the beam. Since the charge orbiting radius is small compared to the waveguide width, the charge location is approximated as the center of the waveguide; this simplifies the calculation of the interaction and is consistent with the other approximations made.

The quantities u_{nx}, u_{ny}, v_{nz}, β_c, ϕ, and τ_n are all "slowly varying" functions of the axial coordinate. Thus over appropriately short distances they can be treated as constant and their derivatives neglected. Substitution of the Fourier expansions into the right-hand side of the wave equations (2,3) yields tractable expressions for the non-homogeneous fields, and completes the self-consistency loop. In the analysis, only terms to order 2ω are retained.

If the transverse non-homogeneous electric field is equal in magnitude and opposite in phase to the transverse homogeneous electric field at the first standing-wave minimum at $z = \lambda/2$, a shorting plane can be introduced and a closed, resonant structure is formed. This condition is imposed as one of the boundary conditions which must be satisfied in the oscillator. Using the definition of "external Q,"

$$Q_x = \frac{\omega \text{ (Stored Energy)}}{\text{Power Out}} , \tag{25}$$

it is found that for this half-wavelength cavity,

$$Q_x = \frac{\omega \ \varepsilon_o \lambda Z_1}{4U} . \tag{26}$$

Fixing the beam kinetic power (VI_o), the strength of the cavity fields is varied by altering the conversion efficiency

$$\psi = \frac{\text{RF Power Coupled Out Through Dielectric}}{\text{Beam Kinetic Power}} = \frac{\frac{E_o^2 a^2}{2Z_1 U}}{VI_o} . \tag{27}$$

Finally, an energy balance factor

$$R(z) = \frac{\text{(Initial Beam Kinetic Power)-(Beam Kinetic Power at z)}}{\text{RF Power Coupled Out Through Dielectric}} \tag{28}$$

is monitored throughout the length of the cavity. Oscillation conditions require the simultaneous existence of two boundary conditions:

$$R(\lambda/2) = 1.0 \tag{29}$$

$$E_{transverse} (\lambda/2) = 0. \tag{30}$$

4. COMPUTATIONAL ASPECTS

The system of the equations of motion (one for each charge group) and wave equations was solved on an IBM 360 digital computer. The cavity and beam parameters were selected to conform as closely as possible to those given by Kulke (1969) for his tube, and are summarized below:

waveguide cutoff frequency	6.56 GHz
cyclotron orbiting frequency	9.35 GHz
beam voltage	15 kV
beam current	5.5 mA
axial velocity	.0181c
transverse velocity	.236c
unmodulated beam diameter/waveguide width	.105

The beam was represented by eight charge groups entering the cavity at intervals of $\pi/4$ in RF phase.

5. RESULTS

Due to uncertainties as to what fraction of the cathode current entered into the interaction process, exact values of saturation beam current for the Kulke oscillator are not available. The tube produced peak power at a loaded Q of 640 and a beam current thought to be about 5.5 mA. At this point, the oscillator efficiency approached 4%. With these parameters as a guide, the model was employed to study oscillator performance at saturation.

With the conversion efficiency set at 1.2%, well below the anticipated saturation level, a sequence of computer runs was made at the 5.5 mA beam current level, while the external Q was varied. As shown in Figure 4, the energy conservation condition of

Equation (29) is satisfied for $Q_x = 351$. The driven RF electric fields at this efficiency level were found to be twice as large as the standing-wave electric field minimum (Figure 5). Holding Q_x fixed at 351, another series of computer runs was made for increasing efficiency levels in order to find the efficiency yielding the short circuit condition of Equation (30). Slight alterations in frequency were necessary at each step to satisfy Equation (29).

Under the influence of the strong transverse RF magnetic field at the cavity entrance, axial accelerations produced charge group crossovers a short way into the structure. Beyond the crossover points, the Fourier expansions of Equation (18) - (20) become invalid as beam velocities are no longer single-valued functions of the axial coordinate. In the face of the extremely non-linear beam response, information on the non-homogeneous field magnitudes must be interpreted with care since these fields are constructed from Fourier coefficients. In spite of the questionability of the Fourier expansions, the analysis was continued beyond the crossing points and led to an interesting and plausible saturation mechanism. Although the computed values of the non-homogeneous fields are dubious, this will not significantly affect the calculation of the charge motion since the non-homogeneous electric fields are very small compared to the homogeneous electric field except near $z = \lambda/2$.

For assumed efficiency levels as high as 13%, frequency alterations could be made to maintain the energy conservation requirement of Equation (29). But as indicated in Figure 5, the limitation on efficiency seems to be set by the inability of the non-homogeneous electric fields to cancel the homogeneous electric field at the standing-wave minimum. Thus the short circuit condition of Equation (30) could not be satisfied. The interaction point in Figure 5 where the non-homogeneous and homogeneous electric fields are equal occurs in the 4½% - 5% efficiency range. With this evidence locating the point of saturation, tube conditions at 5% efficiency were examined in detail.

In Figure 6, the magnitude of the homogeneous transverse standing-wave electric field component is superimposed over the function $\frac{d}{dz}R(z)$ which describes the spatial distribution of the power flux from the beam to the electromagnetic fields.

It is significant that the power exchange is rising rather sharply at the cavity midpoint where the transverse RF magnetic field is at a minimum. If the RF magnetic field were the primary bunching mechanism, the power exchange would level off at the $\lambda/4$ midpoint where B is minimum. The fact that it does not points to the relativistic mass shift as the predominant gain mechanism.

The velocity profiles of the representative charge groups in their flight through the cavity are shown in Figures 7 and 8. It is noted that the maximum increase in transverse velocity gained by beam electrons is about 13%. Since these electrons increase their orbiting radius proportionately, the entire beam remains confined close to the waveguide axis, and at least for the parameters used, collection of charge by waveguide walls does not occur.

The dashed line of Figure 7 shows how the averaged transverse velocity of the beam decreases along the cavity as energy is given to the RF fields. By Equation (1), the average cyclotron frequency is greater than that of the unmodulated beam, and it is anticipated that the oscillation frequency will be above that of the "cold" resonance. Further, the amount of upward frequency shift is limited by beam saturation effects as discussed in Section 2. Steady-state operation sets in at the efficiency level where the saturated beam field matches and cancels the off-resonance field at the output wall (Figure 2b).

It is noted that the averaged axial velocity in Figure 8 tends to remain approximately constant over the entire cavity length. Since energy conversion is at the expense of rotational energy, it is desirable to utilize beams having a high ratio of transverse velocity to axial velocity.

6. CONCLUSION

For X-band frequencies and easily realizable beam parameters, efficiencies on the order of 4 - 5% are predicted for the interaction of a spiraling electron beam with a half wavelength resonant cavity. This prediction agrees favorably with the observed behavior of an existing device (Kulke 1969).

This large signal analysis indicates that the major gain mechanism in the cyclotron resonance oscillator is associated with the bunching produced by changes in mass of the velocity modulated electrons. This effect predominates over the bunching caused by the RF magnetic field. Because the gain mechanism is relativistic in nature, angular velocities of the order of 0.1c must be obtained in the interaction cavity to obtain oscillation.

Essentially, as the output power increases from the start-oscillation condition to the saturated level, the oscillation frequency changes (slightly) to produce the required phase characteristic of the cavity fields relative to the spiraling electron beam. The output power increases until the frequency change is so large that the non-homogeneous RF electric field produced by the modulated electron beam can no longer cancel the homogeneous RF electric field at the collector end of the cavity. At this point, saturation is reached.

The interaction of a spiraling electron beam with a microwave cavity generates intense RF fields which produce strong axial velocity modulation of beam electrons. The electron beam response is extremely nonlinear. Electron crossovers occur within the cavity and a rigorous analysis must account for the multi-valued velocity functions produced on the electron beam.

ACKNOWLEDGMENTS

This work is part of a Ph.D. thesis at Cornell University, supported by the NASA Electronics Research Center, Cambridge, Massachusetts, and guided by Professor Paul R. McIsaac. I remain indebted to Professor McIsaac for the years of direction and aid.

REFERENCES

Antakov, I. I., Gaponov, A. V., Malygin, O. V., and Flyagin, V. A., 1966, Radio Engr. and Elect. Phys., II, 106.

Beasley, J. P., 1966, Proc. Sixth Int. Conf. Microwave and Optical Generation and Amplification, Cambridge.

Bott, I. B., 1964, Proc. I.E.E.E., 52, 330.

Chow, K. K., and Pantell, R. H., 1960, Proc. I.R.E., 48, 1965.

Hirshfield, J. L., and Wachtel, J. M., 1964, Phys. Rev. Lett., 12, 533.

Hsu, T. W., 1966, Ph.D. Thesis, Sheffield.

Kulke, B., 1969, "Design Considerations for Cyclotron Resonance Oscillators," NASA TN D-5237.

Lindsay, P. A., 1970, Proc. Eighth Int. Conf. Microwave and Optical Generation and Amplification, Amsterdam.

McIsaac, P. R., 1968, Proc. Seventh Int. Conf. Microwave and Optical Generation and Amplification, Hamburg.

McIsaac, P. R., and Rowe, J. F. Jr., 1970, Proc. Eighth Int. Conf. Microwave and Optical Generation and Amplification, Amsterdam.

Schriever, R. L., and Johnson, C. C., 1966, Proc. I.E.E.E., 54, 2029.

Sehn, G. J., and Hayes, R. E., 1969, I.E.E.E. Trans. Electron Devices, 16, 1077.

FIGURE CAPTIONS

FIGURE 1. Beam geometry.

FIGURE 2. (a) "Cold" resonance standing-wave patterns; (b) Excited standing-wave patterns.

FIGURE 3. Cavity model and standing-wave pattern.

FIGURE 4. Energy balance factor versus axial distance.

FIGURE 5. Transverse electric field magnitudes at the $\lambda/2$ point versus efficiency. E_{SAT} is the amplitude of the non-homogeneous electric field at $z = \lambda/2$.

FIGURE 6. Axial rate of change of the energy balance factor, $\frac{d}{dz} R(z)$, versus axial position in the cavity.

FIGURE 7. Transverse velocities of the eight charge groups (normalized to the initial DC transverse velocity v_{to}) versus axial position in the interaction cavity.

FIGURE 8. Axial velocities of the eight charge groups (normalized to the velocity of light) versus axial position in the interaction cavity.

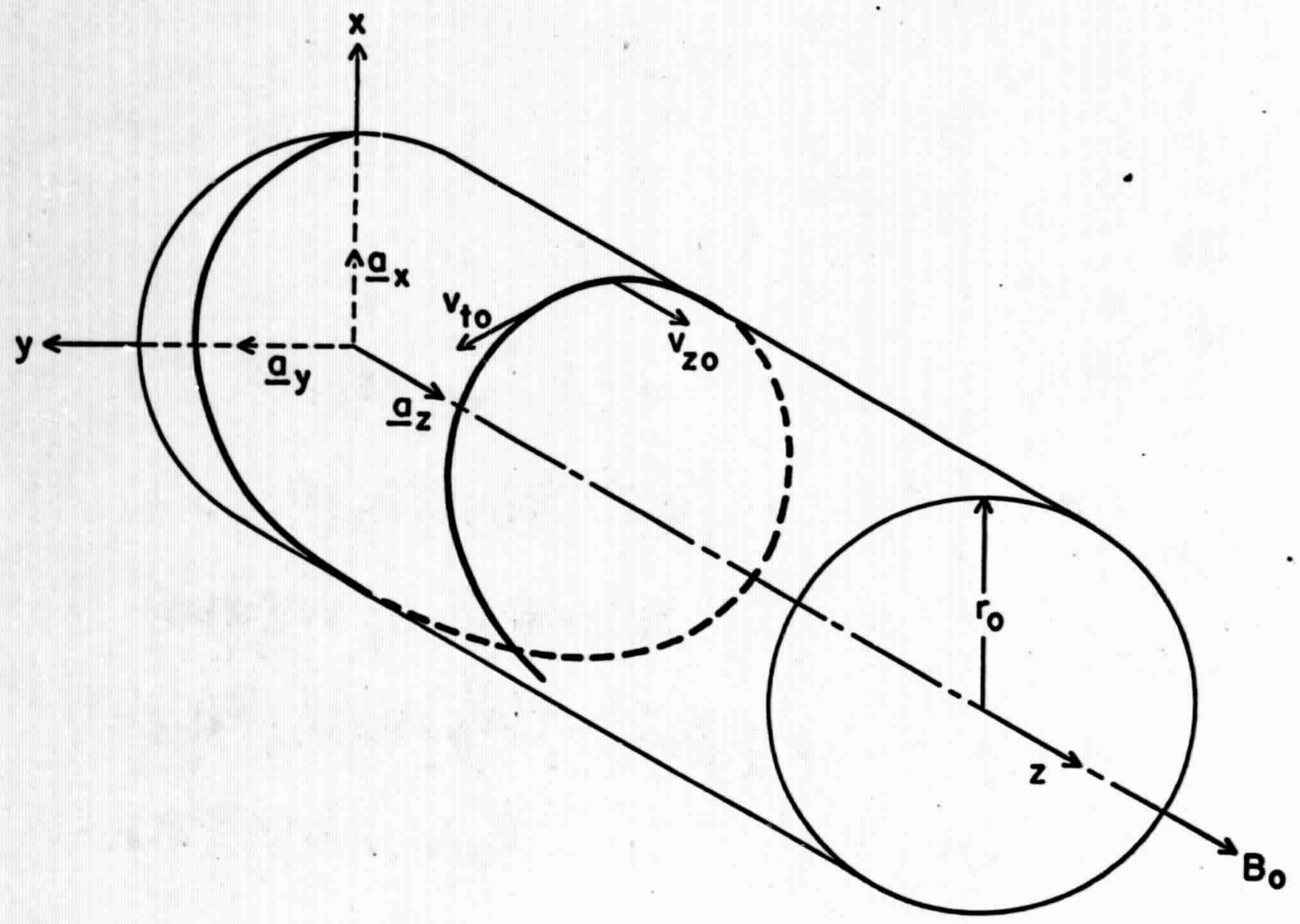

FIGURE 1. Beam Geometry.

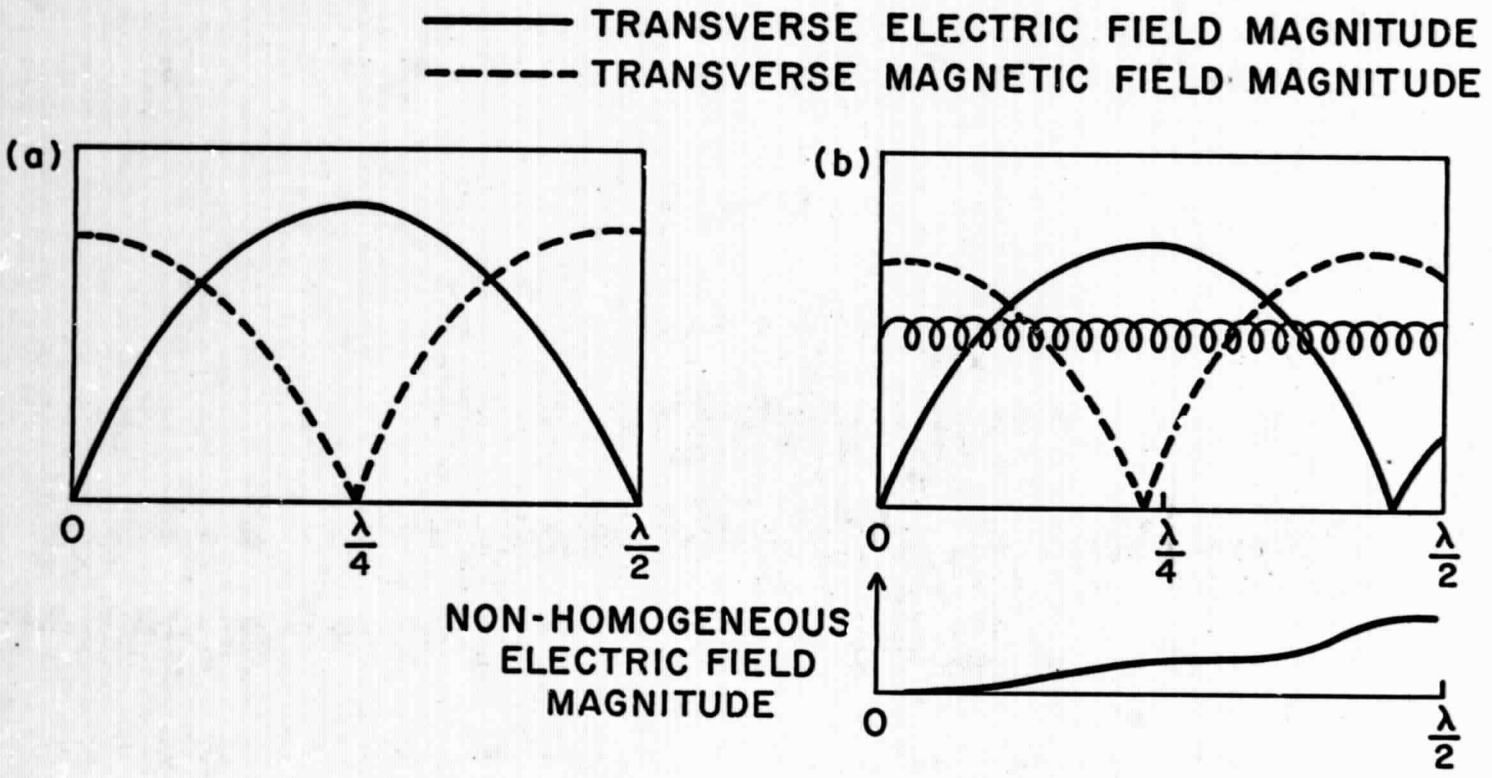

FIGURE 2. (a) "Cold" resonance standing-wave patterns; (b) Excited standing-wave patterns.

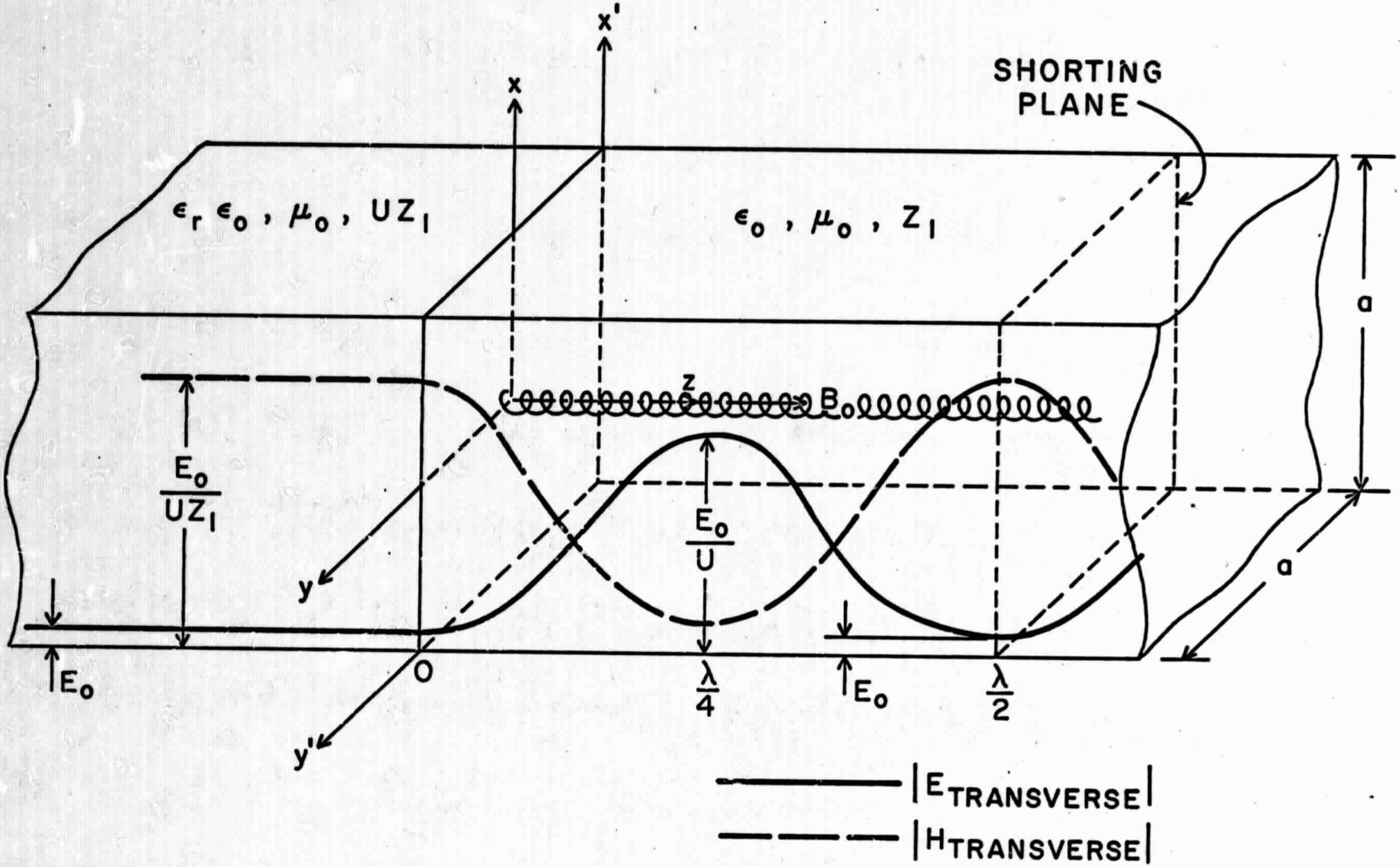

FIGURE 3. Cavity model and standing-wave pattern.

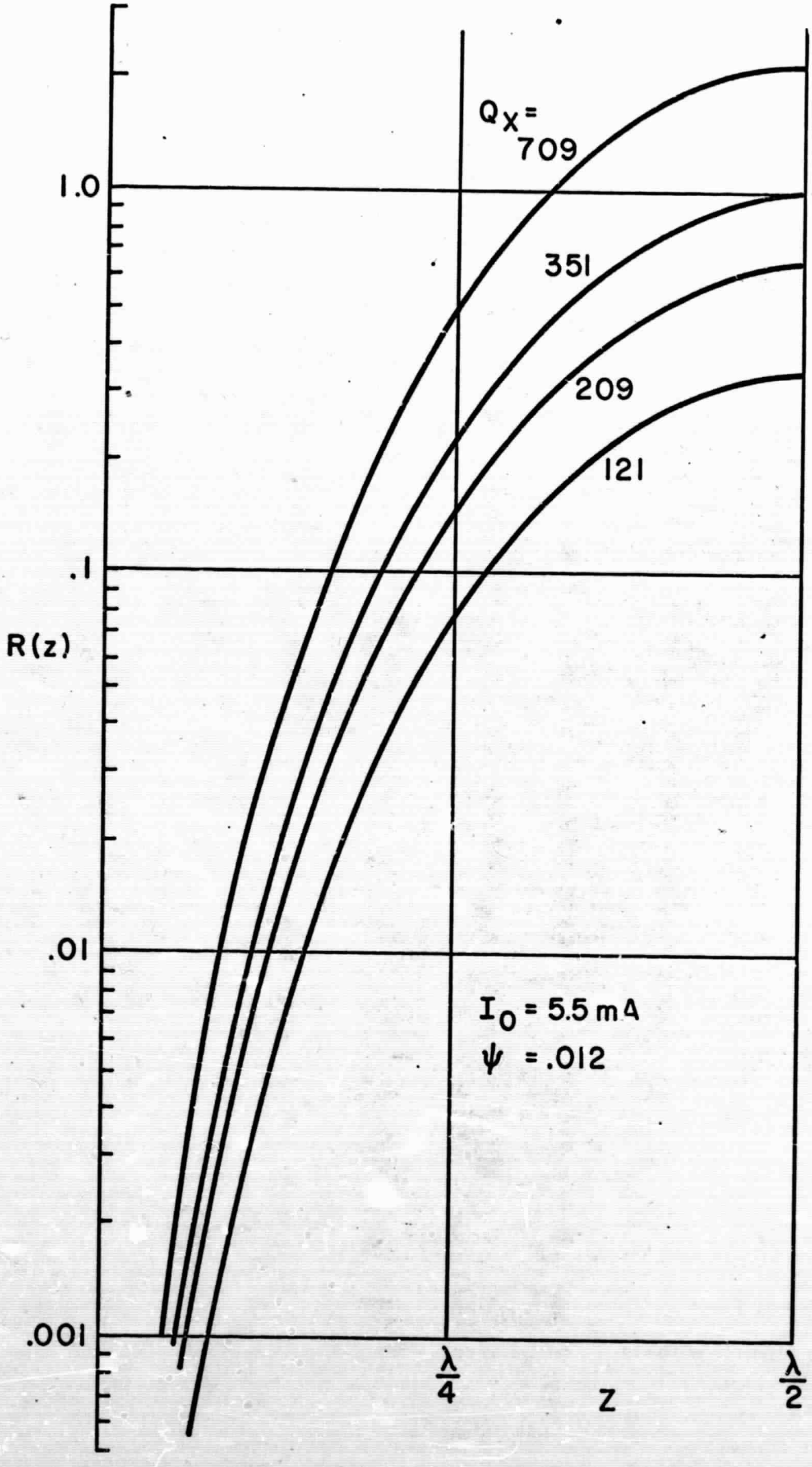

FIGURE 4. Energy balance factor versus axial distance.

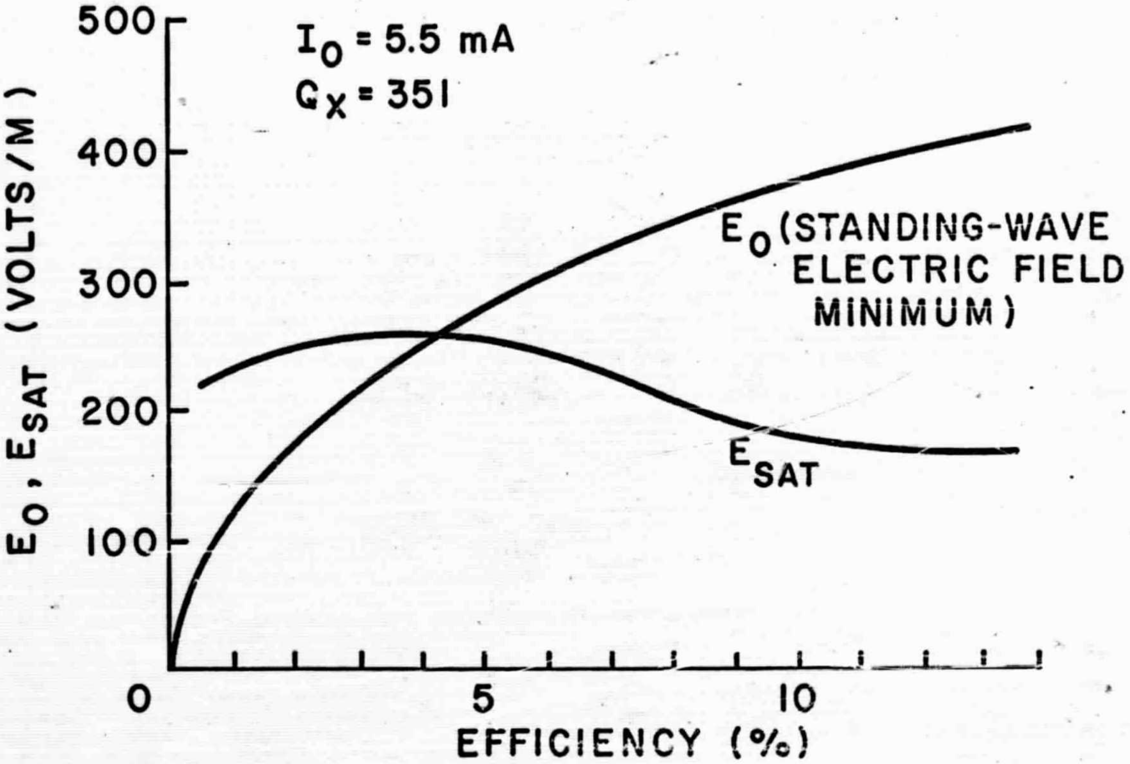

FIGURE 5. Transverse electric field magnitudes at the $\lambda/2$ point versus efficiency. E_{SAT} is the amplitude of the non-homogeneous electric field at $z = \lambda/2$.

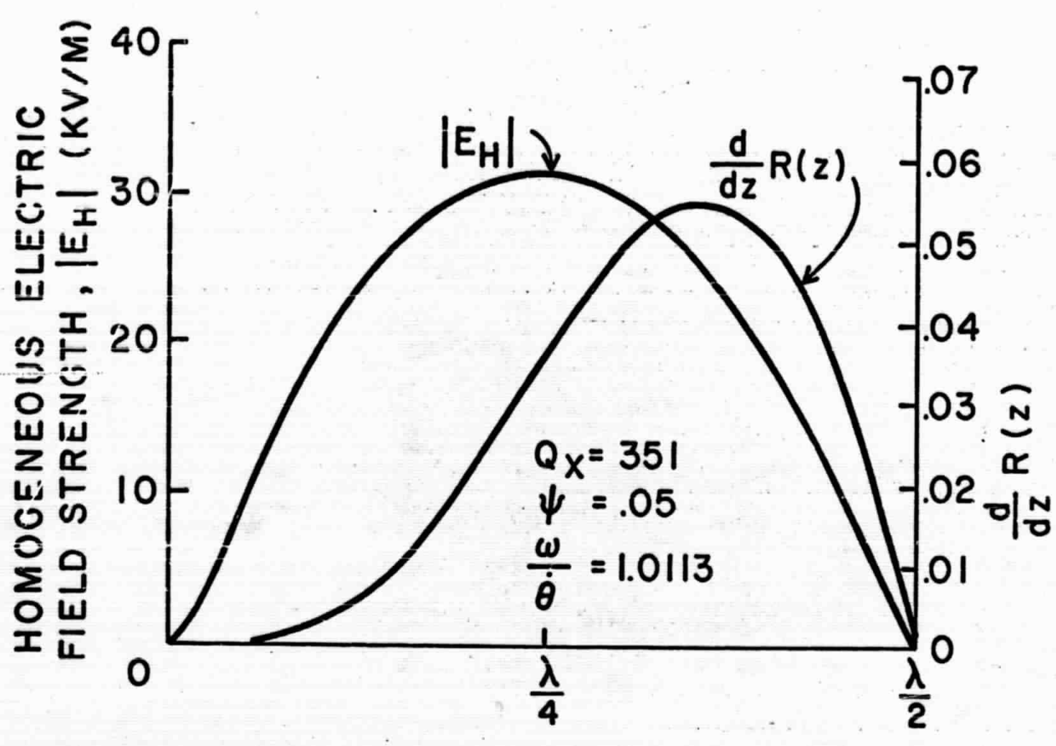

FIGURE 6. Axial rate of change of the energy balance factor, $\frac{d}{dz}$ R(z), versus axial position in the cavity.

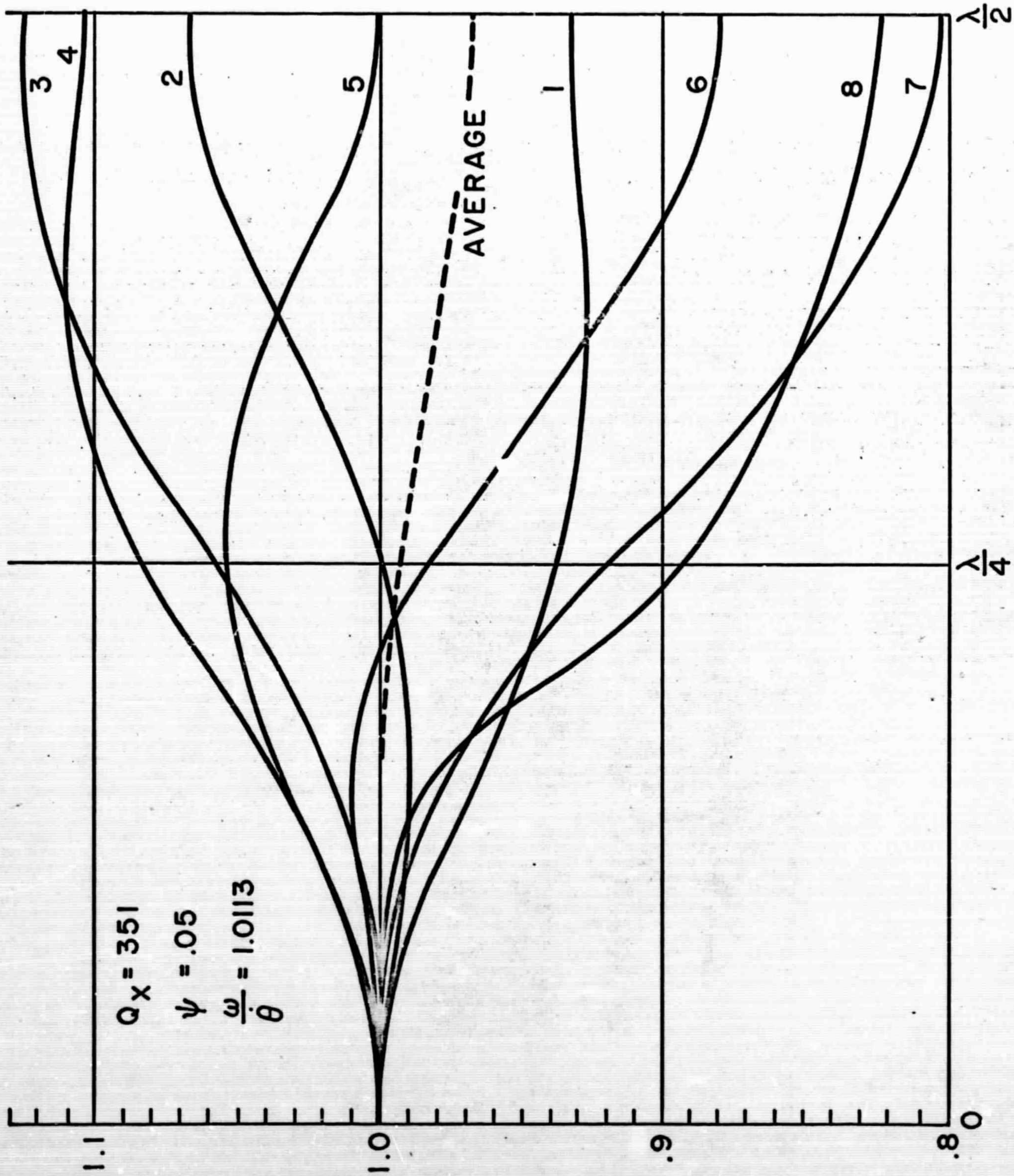

FIGURE 7. Transverse velocities of the eight charge groups (normalized to the initial DC transverse velocity v_{to}) versus axial position in the interaction cavity.

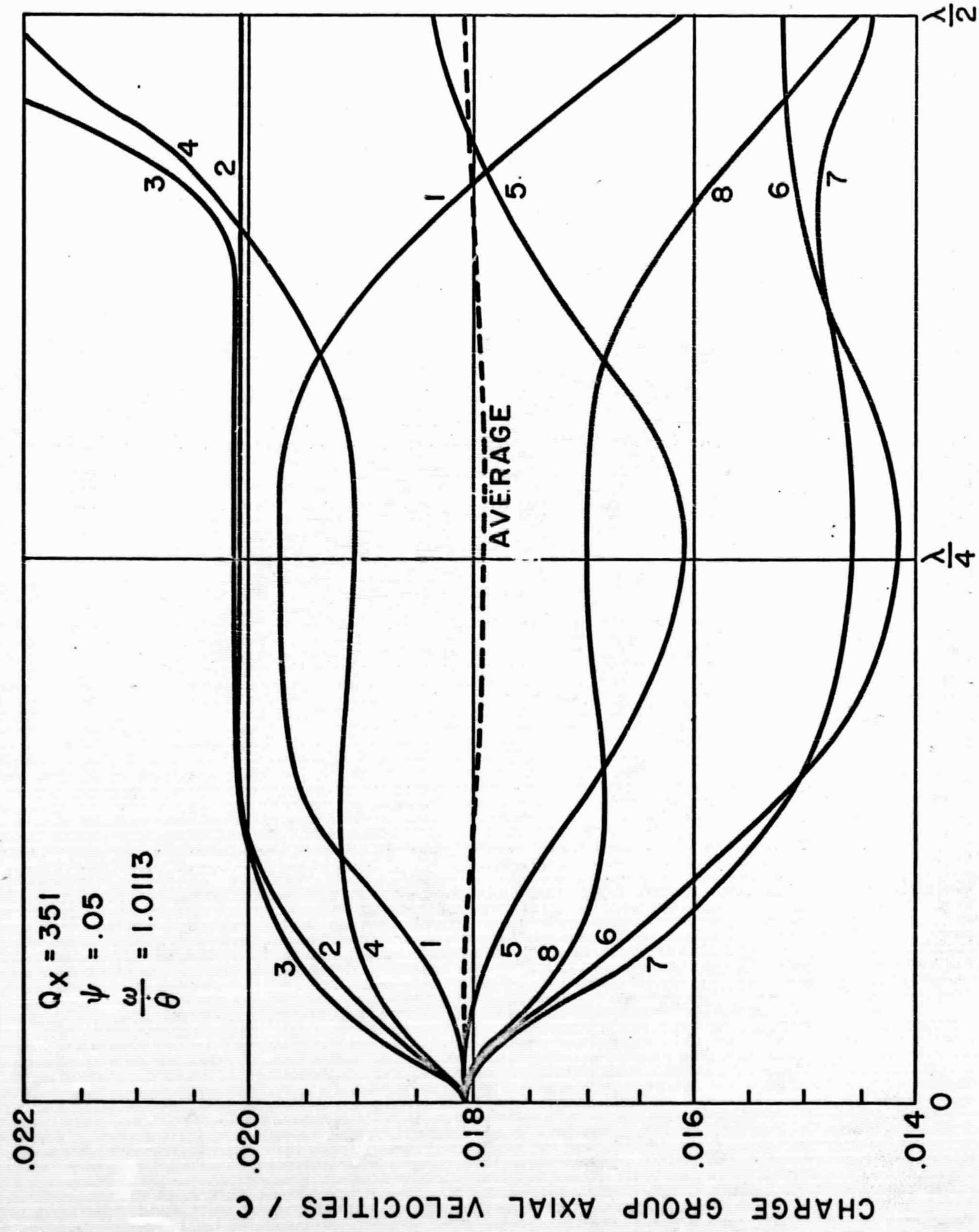

FIGURE 8. Axial velocities of the eight charge groups (normalized to the velocity of light) versus axial position in the interaction cavity).